Agglomerate formation during drying

Alejandro Vertanessian
Department of Materials Science & Engineering, The Pennsylvania State University, University Park, Pennsylvania 16802

Andrew Allen
Ceramics Division, National Institute of Standards and Technology, Building 223/Room A163, 100 Bureau Drive, Gaithersburg, Maryland 20899

Merrilea J. Mayo[a)]
Department of Materials Science & Engineering, The Pennsylvania State University, University Park, Pennsylvania 16802

(Received 1 July 2002; accepted 21 November 2002)

The evolution of agglomerate structure during drying of particles from suspension has been studied for a nanocrystalline Y_2O_3 (8% mol fraction)-stabilized ZrO_2 powder. Agglomerates in drying and dried suspensions were examined at the smallest size scales (1 nm to 1 μm) using ultra-small angle x-ray scattering (USAXS) and at the largest size scales (100 nm to 10 μm) using scanning electron microscopy. The results were correlated with the degree of particle dissolution in each suspension (measured by flame absorption spectroscopy of the suspension filtrate) and the zeta potential of the particles in suspension prior to drying. Results show that large agglomerates readily form across a pH range from 2 to 9. The fact that Y^{+3} ion dissolution varies by over four orders of magnitude in this range leads to the conclusion that there is little direct correlation between the degree of Y dissolution and agglomeration in this system (Zr ion dissolution was below the detection limit at all pH values studied). The observation of large agglomerates well before the introduction of air-water interfaces into the drying mass likewise leads to the conclusion that capillary forces are not essential to agglomerate formation. Instead, agglomerates appear to form as a direct consequence of increasing suspension concentration. Zeta potential also plays a role. Specifically, there was a notable change in agglomerate morphology as the isoelectric point was approached, at approximately pH 8. Here USAXS shows the particles in suspension to have a layered interior structure, with small primary particles aggregated in sheets to form each blocky particle. This is in contrast to the more rounded agglomerates formed away from the isoelectric point, which appear to be composed of the same primary particles arranged in chainlike structures. USAXS of powders from the dried suspensions confirms that the structures seen after drying are the same as those present in suspension. The two structural morphologies are attributed to diffusion-limited (sheets) versus reaction-limited (chains) aggregation, respectively.

I. INTRODUCTION

The formation of agglomerates during ceramic powder processing is a pervasive problem that, in most cases, prohibits the fabrication of fully dense ceramics. Although it is well known that drying of liquid-borne powders will create agglomerates, it is not known exactly how or why those agglomerates evolve in certain size and shape ranges. The problem of agglomeration is particularly acute in the nanometer-size range, where it is argued that both heightened powder dissolution[1,2] and diminishing electrostatic repulsion[3] should make agglomerate formation in drying suspensions the rule rather than the exception. Powder dissolution is envisioned to assist agglomeration through the reprecipitation of dissolved matter at particle contact points, thereby forming interparticle necks.[1] This process would occur primarily during drying of the suspension, as dissolved species become increasingly concentrated and eventually exceed their solubility limit. Electrostatic repulsion, on the other hand, is an original feature of the suspension; it stems from the fact that like-charged clouds of dissolved ions exist around each suspended particle, thereby leading

[a)]Presently adjunct to the Department of Materials and Nuclear Engineering, University of Maryland, Building 090, College Park, Maryland 20742-2115

to mutual repulsion between particles. Agglomeration occurs when the electrostatic repulsion is no longer sufficient to counter the ever-present, attractive London–Van der Waals forces that also exist between particles.

A final mechanism of agglomeration would arguably be the pulling together of discrete particles by capillary forces as air–water interfaces are introduced into a drying mass of particles. The capillary stress on a wettable interface is given approximately by $2\gamma/r$, where r is the cylindrical pore radius and γ is the surface energy associated with the liquid/vapor interface.[4] For pore radii (r) around 5 nm and a roughly estimated surface tension (γ) of 1 J/m^2, it can easily be seen that the capillary stresses in nanoparticulate systems can reach values around 400 MPa. These significant forces are locally compressive on particles at the air–water interface; however, they set up more global drying stresses that are tensile in nature a small distance away from the air–water interface, and that extend deeply (albeit at diminishing stress levels) into the bulk of a drying body.[4] The magnitude of the tensile drying stresses is capped at the magnitude of the capillary force and hence can also reach tens or hundreds of MPa in wet nanoparticulate bodies, especially near the drying front.[4] Thus, during the final stages of drying, one might expect either a pulling together of small particles, due to compressive forces, or the introduction of large cracks into the drying powder, due to tensile forces, depending on whether there existed a cohesive powder unit (e.g., large agglomerate, granule) that was sufficient in size to support a stress gradient.

The present study attempts to distinguish between capillary forces, dissolution and (lack of) electrostatic repulsion as factors in promoting agglomeration by monitoring the evolution in agglomerate size and shape during the drying of suspensions prepared at varying zeta potential and degrees of particle dissolution. For the 8 mol% yttria-stabilized zirconia (YSZ) powders used in the present study, agglomeration due to dissolution and due to zeta potential would be expected to have opposite trends in pH. Dissolution is greatest at low pH (pH 2 and below), so agglomeration would be expected to be greatest at low pH if dissolution is the controlling factor in agglomerate formation. Conversely, the isoelectric point (zeta potential = 0) occurs at high pH in YSZ systems, typically around pH 8. At the isoelectric point, the electrostatic surface charge on the particles is minimized and no longer able to assist in the particles' mutual repulsion while in suspension. Thus, if zeta potential/surface charge is controlling agglomerate formation, agglomeration should be maximized at pH values near the isolectric point, i.e., at high pH. Finally, if agglomeration is not pH dependent and does not appear until the final stages of drying—when an air-water interface begins to intrude into the drying mass—then capillary forces are the most likely culprit.

To detect the agglomerates as they form during drying, ultrasmall angle x-ray scattering (USAXS) was used, which can conveniently probe 1 nm to 1 μm agglomerates in both wet and dry states. For confirmation, scanning electron microscopy (SEM) was also conducted both on agglomerates extracted from suspension and on agglomerates dried from suspension. In both cases, SEM examines agglomerates in the dried state.

II. METHODS AND MATERIALS

A. Powder preparation and characterization

YSZ nanocrystalline powders (8 mol%; 8 nm crystallite size) were produced by an aqueous chemical precipitation technique, the details of which have been presented previously.[5] However, more yttria was incorporated into the stock solution, corresponding to an increase from 3 mol% yttria doping[5] to 8 mol% yttria doping for the present study. Fourteen separate double batches of nanoparticulate 8 mol% YSZ were prepared and then mixed together into a single homogeneous batch of 0.2 kg. Homogenization was performed by ball milling the powder with no balls and no additives for 24 h, i.e., by rotating the powder in a plastic (HDPE) container in a roller mill. All experiments were conducted on samples drawn from this one 0.2 kg batch of powder.

X-ray diffraction (XRD) of as-prepared powder was performed to measure crystallite sizes using the Scherrer technique[6] applied to the [111] peak of the cubic zirconia phase. Cu K_α radiation was used in a Scintag PAD V x-ray diffractometer (Scintag, Cupertino, CA). Crystallite size was also calculated from Brunauer–Emmett–Teller (BET) surface area measurements of the powder using nitrogen gas in a Micromeritics ASAP 2010 BET instrument (Micromeritics, Norcross, GA).

To characterize the powders in their initial suspended state, SEM was performed using a Philips XL-20 (Eindhaven, the Netherlands) electron microscope. Samples of suspended powders were prepared for SEM by dipping a highly polished Al sample holder for 10 min into a 1% mass solution of polyacrylamide, rinsing with distilled water, then dipping for 1 min into a pH 2, 8, or 9 suspension containing 0.06% by mass of nanocrystalline YSZ, rinsing with distilled water, then air drying. The suspensions were ultrasonicated for 12 h in an ultrasonic bath prior to sampling. This procedure allows the sample holder to "capture" individual suspended particles in the suspension, and prevents the particles from subsequently moving during drying. Thus, a more accurate picture of the particles as they exist in suspension is achieved than can be obtained by more standard SEM preparation methods.

B. Dissolution measurements

For the dissolution experiments, 2.4% by mass suspensions of YSZ in doubly distilled deionized (DDI) water were prepared of pH 2 and 3.5 using HNO_3 as the pH-adjusting additive; basic suspensions of pH 6, 8, 9, and 10 were prepared using NH_4OH as the pH-adjusting additive. A final pH adjustment was performed after the powder was added, and the suspension sat for 5 min under magnetic stirring. After the final pH adjustment, the suspensions were agitated with an ultrasonic horn (50% duty cycle and 50% full power; Branson Ultrasonics Corporation, Danbury, CT) for 5 min to ensure full mixing. Dissolution was then measured as a function of time using a syringe with a 20 nm membrane filter (Nuclepore membrane, Whatman Inc., Tewksbury, MA) to extract the solvent from a given particulate suspension at time intervals ranging from 0 h (just after ultrasonication) to 100 h. Suspensions were continuously stirred by a magnetic stirrer during the time interval over which samples were taken. After extraction, the particle-free liquid was analyzed by inductively coupled plasma emission spectroscopy (Model PS3000UV from Leeman Labs Inc., Lowell MA) to detect the presence of dissolved cations. Measurements were made with reference to Y standards of 5, 2, and 0.1 parts per million and to similar Zr standards.

C. Zeta potential

The zeta potential of the YSZ powder was obtained from mobility measurements as a function of pH using a Beckman Coulter Delsa 440SX instrument (Beckman, Miami, FL). The variations in pH, from pH 2 to pH 9.5, were achieved by adding either nitric acid or ammonium hydroxide to the suspensions being measured. Suspensions used for zeta potential measurements contained 0.01% by mass powder in DDI water and were ultrasonicated 12 h in an ultrasonic bath prior to measurement.

In a separate set of experiments, zeta potential was measured in 0.01% powder suspensions by mass for which the liquid medium was not DDI water, but rather particle-free filtrate taken from more concentrated suspensions (37.5% powder by mass) by syringe (20 nm filter) extraction after 2 h. The purpose of the latter experiments was to emulate the solution conditions found in USAXS measurements, where sample preparation generally involves higher powder loadings and thus results in higher ionic strengths of the surrounding suspension, due to concurrent powder dissolution. The zeta potential measurements made with the higher ionic strength liquid were conducted at pH 2, 8, and 9 after bath-type ultrasonication of the suspensions for 2 to 3 h. Either a Brookhaven PALS Zeta Plus Analyzer (Brookhaven Instruments, Holtsville, NY), for pH 8 and 9 measurements, or a Beckman Coulter Delsa 440SX for pH 2 measurements was used for these experiments.

D. SEM of powders from dried suspensions

Dried powders were also viewed by SEM**.** Suspensions were first prepared by adding 37.5% powder by mass to DDI water preadjusted to pH 2, 8, or 9. Suspension pH was readjusted slightly after the introduction of the powder. Nitric acid (pH 2) and ammonium hydroxide (pH 8 and 9) were used as the pH-adjusting agents. The suspensions were allowed to dry completely under ambient conditions, and the dried cakes were broken with a spatula to obtain the dry powder. The powder was then sprinkled over a wet colloidal Ag layer on a polished Al sample holder and the Ag paint was allowed to dry. An Au coating was then sputtered on to all powder SEM specimens prior to viewing.

E. USAXS

USAXS was used to examine the finer features of agglomerate structure during the drying of the suspensions. Suspensions for USAXS were prepared in a similar manner to those for dissolution experiments, except the solids loading in the suspensions was 37.5% by mass (9.1% by volume), suspensions were agitated for 1 h using an ultrasonic cleaner, and only samples of pH 2, 8, and 9 were examined. USAXS samples of pH 2 and 9 were of three types: suspension, suspension air-dried to paste consistency, and suspension air-dried completely. At pH 8, only two types of samples could be prepared due to the limited powder remaining: fresh suspension and suspension air-dried completely (i.e., fully dried).

The fresh suspensions and partially dried pastes for USAXS measurement were mounted in individual liquid cells specially designed for small-angle x-ray scattering studies. The cell design provides a suitable geometry for x-ray incident beam entrance and scattered beam exit, and secures the sample between parallel layers of polyimide film separated by a 1.00-mm x-ray flight path through the sample. To ensure that the irradiated sample volume was representative, a suspension drop or paste pellet was placed within the partly-assembled cell and the cell assembly then completed around the sample. For the fully dried samples, the powder residue was secured between adhesive layers of polyamide tape and the effective sample thickness was determined from micrometer measurements.

The USAXS measurements were carried out using the double-crystal Bonse–Hart small-angle x-ray scattering method[7] at the UNICAT USAXS facility,[8] sector 33, Advanced Photon Source, Argonne National Laboratory, Argonne, IL. Raw data were collected as scattered intensity versus the magnitude Q of the scattering vector

Q where $Q = (4\pi/\lambda) \sin(\Phi_S/2)$, Φ_S being the angle of scatter out of the incident beam direction and λ the wavelength of the incident x-ray beam. In its standard form, USAXS instrument data are intrinsically slit-smeared but can be desmeared using a well established algorithm by Lake.[9] The desmeared scattered intensity, $I(Q)$, versus Q data were then analyzed using an entropy maximization method, MaxEnt[10] to determine the primary particle size distributions in the suspensions, pastes, and dried residues. The Porod Q^{-4} terminal slope of the scattering at high Q was also analyzed to determine the particle surface area per unit solid volume[11] in the suspensions and pastes. Finally, of most interest in the present study, the scattering curves were inspected to determine the various agglomeration morphologies present, as a function of length-scale.

III. RESULTS AND DISCUSSION

A. Characterizations of starting powders

Initial powders were of nanocrystalline particle size, as can be seen from the SEM micrographs of particles captured from pH 2, 8, and 9 suspensions [Figs. 1(a), 1(b), and 1(c), respectively]. Particles from all suspensions look approximately the same in SEM, with the bulk of the (number-based) distribution appearing to be particles in the diameter range of 10–50 nm. In each case, the particles were composed of even smaller crystallites, as evidenced by the fact that XRD and BET measurements of crystallite size for this powder give values of 8.1 and 9.34 nm, respectively, while MaxEnt size distribution analysis of the USAXS data suggests a primary particle diameter in the range 7 to 8 nm. Thus, the starting powder is already agglomerated on a small scale, prior to drying of the suspension.

B. Dissolution measurements

Dissolution experiments show that Y from the powder dissolves very rapidly—typically within the first 15 min after the sample is made (Fig. 2). The degree of dissolution is very high at low pH with approximately 35% of all Y in the powder dissolving at pH 2. The degree of dissolution decreases monotonically until it reaches less than 0.05 μg/g (under the detection limit of the spectrophotometer), at pH 8 and 9; see Figs. 2 and 3. Zr dissolution was virtually nonexistent at all pH values, measuring 0.02 μg/g or less. The statistical uncertainty in dissolution measurements was assumed to be the order of 1–2%, in keeping with the typical uncertainty for this technique[12] or on the order of the detection limit (0.02 μg/g for Zr ions and 0.05 μg/g for Y ions), whichever was larger for the measurement in question.

The dissolution results are entirely consistent with the published solubility predominance diagrams for yttria and zirconia,[13] which show a solubility minimum for yttria at pH 9 to 10, and even lower solubilities for zirconia across the entire pH 2 to 10 range. In the present study, the four orders of magnitude decrease in solubility for Y (from 952 μg/g at pH 2 to 0.05 μg/g at pH 8–9)

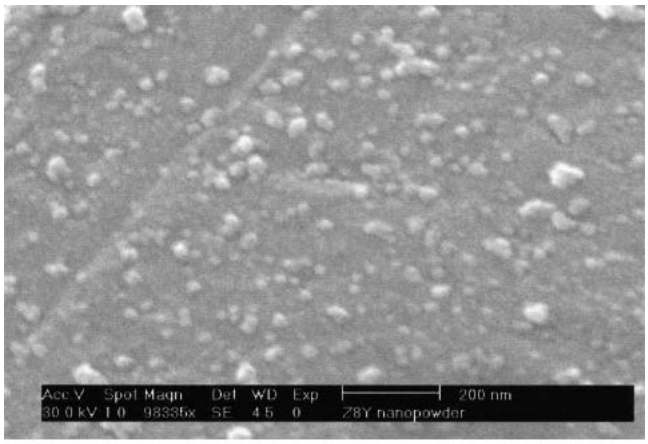

(a)

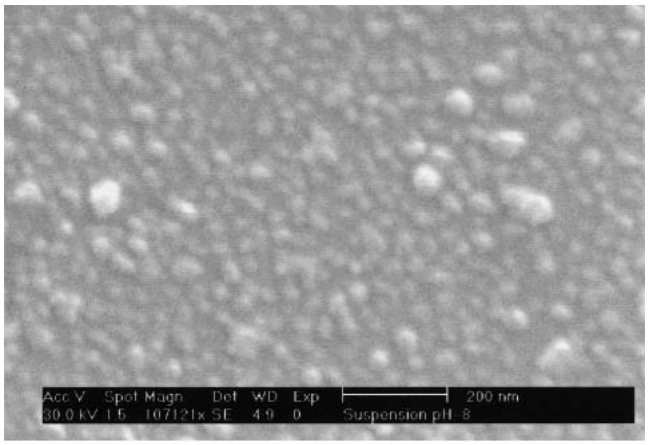

(b)

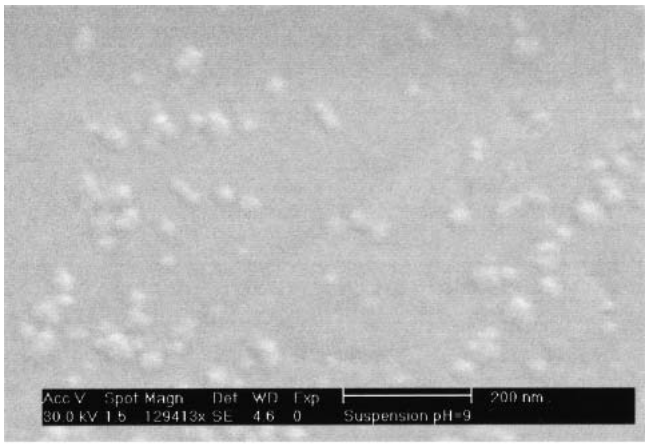

(c)

FIG. 1. SEM images of nanocrystalline YSZ powder dispersed in (a) pH 2, (b) pH 8, and (c) pH 9 water and attached to an Al surface previously covered with polyacrylamide. Scale markers correspond to 200 nm in each case.

allows the preparation of powders that have experienced distinctly different levels of dissolution, a necessary first step in determining whether dissolution of fine powders plays a role in their agglomerate formation.

C. Zeta potential

Zeta potential measurements on low ionic strength suspensions indicate the isoelectric point of the nanocrystalline YSZ powder is at approximately pH 8.6 (Fig. 4). However, the instrument used demonstrated high variability in its readings at pH 8, making that particular data point uncertain. This in itself suggests the isoelectric point may be closer to pH 8 than pH 9.

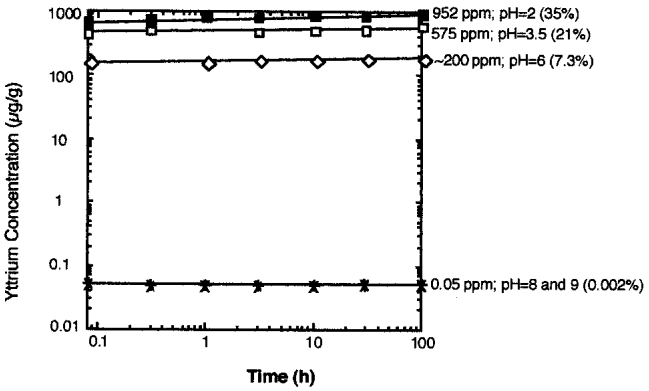

FIG. 2. Sample dissolution data for nanocrystalline YSZ particles. Data in parentheses indicate percentage of total Y in the powder that was dissolved at 100 h. The statistical uncertainty in dissolution measurements was assumed to be the order of 1–2%, in keeping with the typical uncertainty for this technique[11] or on the order of the detection limit (0.02 μg/g for Zr ions and 0.05 μg/g for Y ions), whichever was larger for the measurement in question.

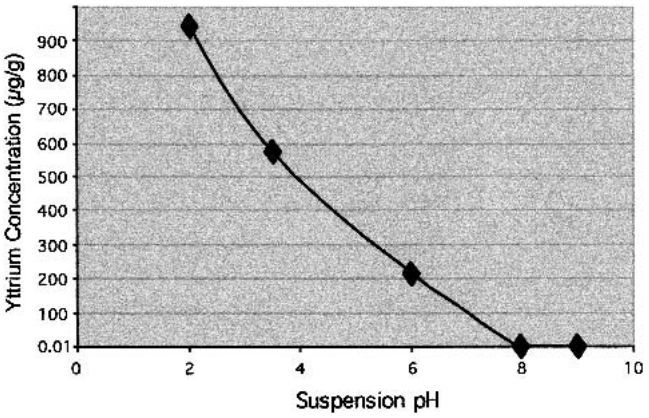

FIG. 3. Equilibrium (100 h) values of dissolved Y (μg/g) at different pH values. The statistical uncertainty in dissolution measurements was assumed to be the order of 1–2%, in keeping with the typical uncertainty for this technique[11] or on the order of the detection limit (0.02 μg/g for Zr ions and 0.05 μg/g for Y ions), whichever was larger for the measurement in question.

Aside from pH 8, the variability in zeta potential measurements was in the 5–10% range, based on three measurements per suspension.

Zeta potential measurements using high ionic strength suspensions (i.e., taken using small amounts of powder suspended in liquid filtered from concentrated suspensions) yielded zeta potentials near 0 in every case examined (data not shown in Fig. 4). At pH 2, 8, and 9, the zeta potentials were 2.3, 3.11, and –1.95 mV, respectively. This result illustrates the role that dissolved ions play in shielding the surface charge around the particles. For example, there should be a significant detectable charge on particles at pH 2, but because there are so many dissolved ions in suspension at this pH, no long-range charge can be detected by the instrument through the "screen" set up by these ions. At pH 8 and 9, there are far fewer dissolved cations, but chloride-derived powders typically release residual Cl^- anions from their surface when put into suspension,[14] and these may contribute to charge screening as well. The exact ionic makeup of these suspensions is not known. However, it is likely the concentration of $[Y^{+3}]$ for the concentrated pH 2 suspension is in the 10^{-1} to 1 M range. A linear extrapolation of the dissolution data to the higher solids loadings would predict a 0.256 M concentration, and dissolution of all yttrium in the powders would lead to a maximum limit of a 0.85 M $[Y^{+3}]$ in solution for the present case. (Note the 0.85 M value is still well below the solubility limit[13] for $[Y^{+3}]$ at pH 2). For the pH 8 and 9 suspensions, the solubility limits[13] for $[Y^{+3}]$ are quite low, between 10^{-7} and 10^{-9} M, so the most likely contributor to charge screening would be spurious Cl^- ions. Though such ions may play a secondary role in modifying interparticle electrostatic forces, they are not expected to directly contribute to interparticle neck formation by reprecipitation of Cl-containing compounds, which tend to be either liquid or volatile. (Certainly parallel differential scanning differential calorimetry experiments showed no evidence of Cl-containing compounds in dried powders—solid, liquid, or otherwise[15]).

With respect to the USAXS measurements, which were conducted at high powder loadings and thus equivalently high ionic strengths, the zeta potential results in high ionic strength (but dilute particle number) suspensions implies that only short-range interparticle forces will be acting. Since these are precisely the forces likely to contribute to agglomeration, it is likely that agglomeration will be more prominently observed in the USAXS suspensions, which have higher ion concentrations than in the more dilute suspensions prepared for SEM and zeta potential measurements.

The null zeta potential result also has implication for suspensions dried in the laboratory, which undergo increasing ion concentration as liquid is removed from suspension. In these, too, there will be few long-range

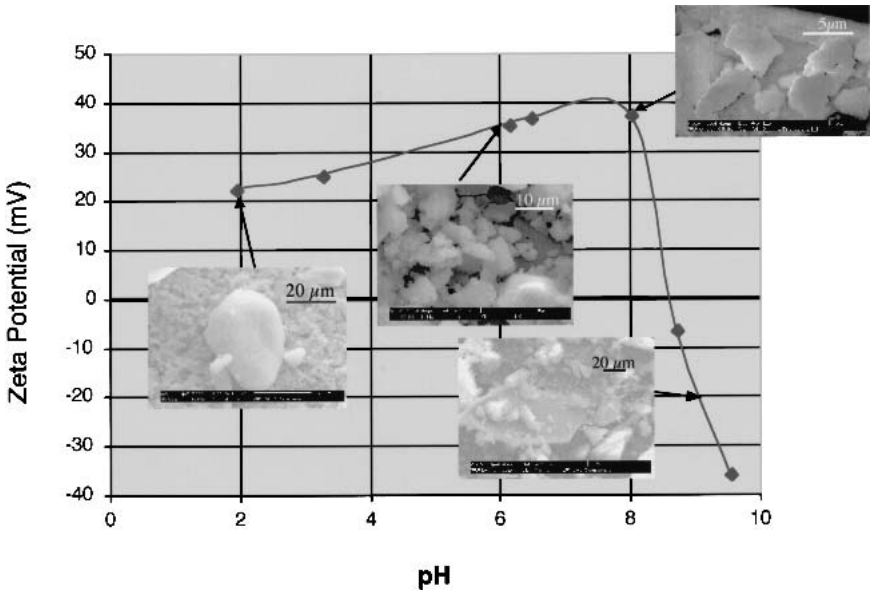

FIG. 4. Zeta potential versus suspension pH for nanocrystalline YSZ powder. SEM micrographs of the agglomerate shapes resulting from suspension drying are shown for pH 2, 6, 8, and 9. Aside from pH 8 (where the measurement was erratic), the variability in zeta potential measurements was in the 5–10% range, based on the three measurements per suspension, whose average is shown here. Scale markers in upper right of micrographs represent 20 μm at pH 2, 9, and 10 μm at pH 6, and 5 μm at pH 8.

electrostatic repulsive forces to prevent agglomeration—increasingly so the suspensions become more and more concentrated throughout drying.

D. SEM of powders from dried suspensions

From SEM of completely dried suspensions, it is apparent that the small aggregates present in the original suspension (Fig. 1) grew significantly upon drying (Figs. 4 and 5). However, there are two germane features of the agglomerates in the dried state. First, many large agglomerates are present, regardless of pH, covering a wide size distribution in the 1–50 μm range. This result argues against dissolution playing the dominant role in agglomeration. Recall that the extent of Y dissolution varies over four orders of magnitude between pH 2 and pH 8–9, yet large agglomerates are just as prevalent at pH 8–9 as they are at pH 2. The agglomerates appeared to be slightly larger at pH 2 versus pH 8–9; however, the shapes of the agglomerates are also sufficiently different that a strict size comparison is not particularly meaningful.

This brings up the second point, namely, that there is a dramatic change in the shape of the agglomerates around the isoelectric point (pH 8–9). Far from the isoelectric point, (pH 2–6), the agglomerates are large globules composed of small equiaxed crystallites. Close to the isoelectric point (pH 8–9), the same crystallites are arranged in sheetlike structures, which then stack to make plate and/or block-shaped agglomerates. The layered structure is most acute at pH 8, but is also present to a lesser degree at pH 9.

The significant change in agglomerate morphology as a function of pH has repercussions for compaction and subsequent sintering of suspension-dried powders. This point has been discussed previously in some detail,[15–17] where it was shown that the blocky-type agglomerates compact poorly and yield low green densities compared to rounded-type agglomerates,[15,16] even when the latter are measurably stronger.[15]

E. Small-angle scattering measurements

Figure 6 shows the absolute-calibrated, de-smeared USAXS intensities versus Q for samples in various stages of drying. On the log–log scale plotted, all of the data sets—pH 2, 8, and 9—have a similar overall shape as a function of Q, which is found not to vary significantly over the wide suspension concentration range actually sampled within the x-ray beam. This extends from around 3% by volume where particles have dropped out of suspension up to nearly 25% by volume for the settled-out particle concentration. However, significant differences exist within each of the three distinct regions observed as a function of Q. While some similarities exist with the data obtained for various hierarchical structures found in polymer systems, the microstructural models developed for such systems[18] are not appropriate for building an understanding of the nanoparticulate agglomeration problem studied here. Thus, most of our comments are confined to what can be learned from the USAXS data by direct inspection.

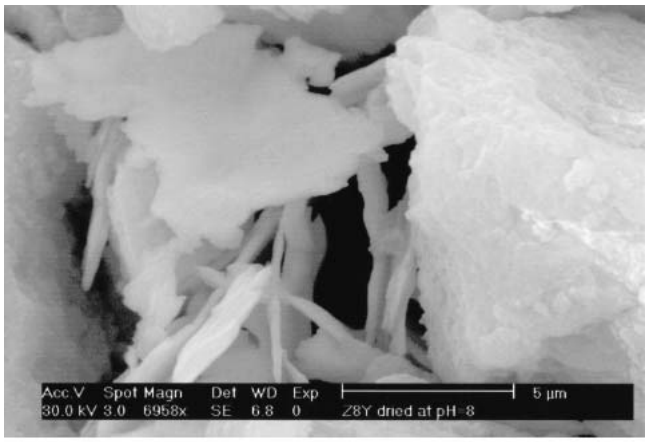

(a)

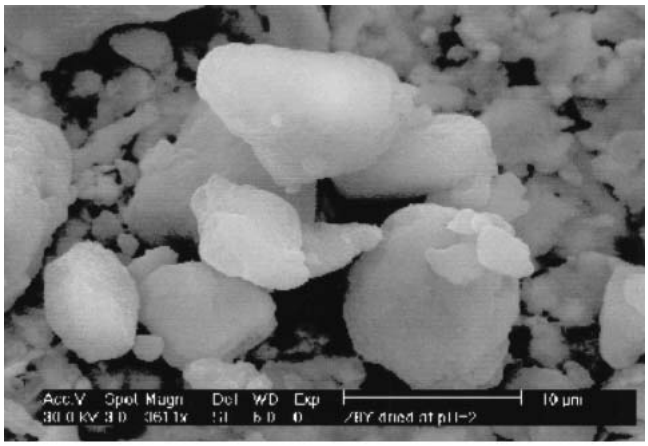

(b)

FIG. 5. Large agglomerates at (a) pH 8 and (b) pH 2, showing the difference in structure near and far away from the isoelectric point, respectively. pH 8 agglomerates reflect an internal platelike structure, while the pH 2 agglomerates are composed of more globular aggregates.

1. Small-scale agglomerate structure

For the USAXS data at $Q > 0.7$ nm^{-1} (smallest particle sizes) behavior close to a Q^{-4} power law is observed. An exact Q^{-4} behavior would be characteristic of the Porod scattering[10] from the surfaces of discrete Euclidean shapes, consistent with the concept of crystallites as the smallest powder units. For the fresh suspensions of pH 2 and 9, the slope is steeper than Q^{-4}: –4.8 ± 0.1, where the standard deviation is deduced from power law fits to the data from several samples. This suggests a diffuse gellish nature to the surface of the primary particles. For the partially dried suspensions the exponent is closer to four: 4.4 ± 0.1, and true Porod scattering with an exponent of 4.0 ± 0.2 is observed for the fully dried suspensions. However, at pH 8, the exponent for the fresh suspension is 4.0 ± 0.1, indicating that a sharp particle interface already exists for the fresh suspension where the pH is close to the isoelectric point.

There is interesting circumstantial evidence that suggests that the "gellish surfaces" seen (or not) by small-angle x-ray scattering (SAXS) may actually be the electrostatic double layer of ions that surrounds each primary particle in suspension. In some sense, the layering of dissolved high atomic number Y^{+3} ions next OH^- ions in an extended double layer (or the layering of more complex species containing the above elements) would not be that different from the Zr(Y)–O nearest neighboring in the solid. A SAXS study would interpret the alternate layering of high atomic number and low atomic species in suspension as a diffuse interface (Q exponent greater than 4), rather than a rough interface (Q exponent less than 4), simply because of the atomically fine scale of the mixing. However, the most compelling evidence that the diffuse crystallite surfaces seen in SAXS somehow relate to the existence of the crystallites' double layer is that the observed changes in gellishness under different suspension conditions correlate strongly with the expected changes in double layer width, under those same conditions. For example, the most diffuse interface is observed by SAXS away from the isoelectric point and under dilute suspension conditions, where the double layer is known to be thick (large Debye length)[19]; the degree of gellishness or diffuseness becomes increasingly less as the suspension dries—conditions under which the double layer should shrink, because the ionic concentration of the suspension is increasing (small Debye length)[19]—and, finally the diffuse interface fully disappears in SAXS once the suspension is completely dried (no double layer) and/or the suspension is at the isoelectric point (also minimal to no double layer).

In addition to the rather intriguing gellish interface issue, SAXS also reveals information on particle size scales for the smallest structural units (crystallites). Transition to the final Porod Q^{-4} regime (smallest particles) occurs at around the same Q in all powders, suspended or dried, indicative of a common fundamental particle size. This is confirmed by the MaxEnt size distribution analyses,[10] which consistently show a primary particle population with a mean diameter in the range 7 to 8 nm for all powder and suspension samples. This is broadly consistent with the XRD data (8.1 nm) although it is a slightly smaller value than given by BET (9.34 nm).

For MaxEnt size analyses, absolute calibration of the volume fraction size distribution is based on x-ray scattering contrast: $|\Delta\rho|^2 = 1107 \times 10^{28}$ m^{-4} between YSZ and H_2O, with an assumed YSZ density: 6.0 g cm^{-3}. Discrete spherical particles are assumed, and so the MaxEnt size distributions do not give valid quantitative information on the large-sized agglomerates. However, the total solid volume fraction can be estimated by integrating the MaxEnt size distribution over the size range. The total surface area per unit sample volume S_T of each

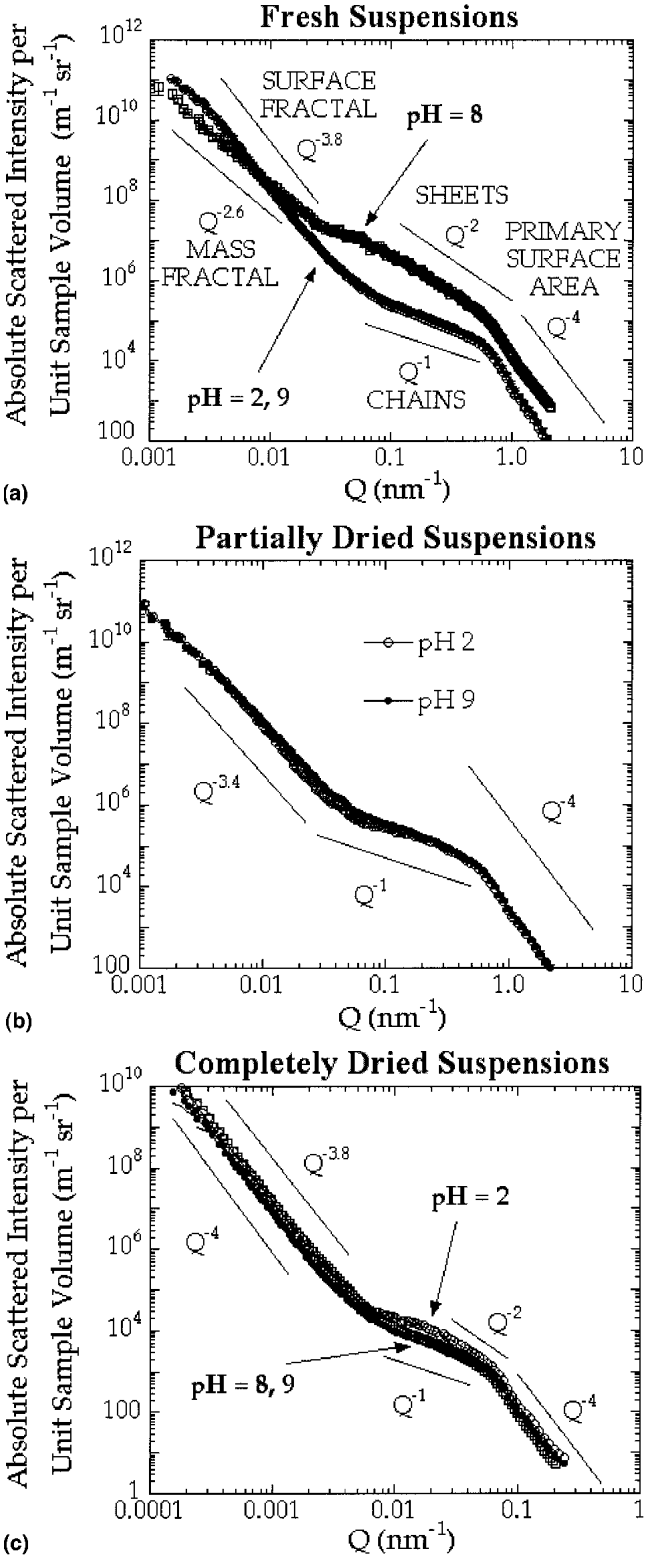

FIG. 6. USAXS data versus Q with fits obtained using MaxEnt size distribution algorithm. "Noise" in data is indicative of data uncertainties and is consistent with computed standard deviations where these are given by vertical bars for (a) freshly made suspensions, (b) suspensions dried to a paste consistency, and (c) suspensions dried completely. Power law gradients are given as guides to the eye and are discussed further in the text.

suspension can also be estimated by force-fitting a Porod Q^{-4} scattering power law[10] to the data at $Q > 0.7$ nm^{-1}, and then applying Porod's law: $I(Q) = 2\pi|\Delta\rho|^2 S_T/Q^4$. Based on the results for four separate suspensions, the surface area and its standard deviation for the fresh suspensions is (137 ± 5) m^2 g^{-1}, for partially dried suspensions it is (159 ± 4) m^2 g^{-1}, and for fully dried suspensions it is (149 ± 13) m^2 g^{-1}. These values are 5–15% higher than would be expected for smooth spherical primary particles, suggesting that either departure from spherical shape or surface roughness increases the specific surface areas. However, both particle agglomeration and the existence of a diffuse interface should decrease the measured specific surface areas. These latter two effects compete with the former two and their variation probably accounts for the modest changes in specific surface area as drying proceeds.

On combining the above data, the specific surface area per unit solid mass in the suspensions is found to be virtually independent of the suspension concentration. This implies that "welding" of particles in the literal sense, or substantial filling in of interparticle necks by dissolved + reprecipitated material, does not occur as drying takes place. Otherwise, a surface area decrease on the order of 22%, corresponding to the formation of an equilibrium interparticle neck geometry,[20] should have been observed.

2. Intermediate scale agglomerate structure

At intermediate Q (0.07 nm^{-1} < Q < 0.7 nm^{-1}), data adhere to a power law dependence between Q^{-1} and Q^{-2}, suggesting some organization of the primary crystallites into chains (Q^{-1}) and sheets (Q^{-2}).[11] Exponents between one and two can occur if chains curl up into coils or if sheets are significantly holed. Some mixing of chain- and sheetlike structures is also likely. The scale range over which the chain and/or sheetlike structure exists extends from slightly under 10 nm (to give Porod scattering for $Q > 0.7$ nm^{-1}, consistent with the thickness of the chain or sheet being the primary particle size) up to 80 to 90 nm for the chain length or sheet diameter (to give the observed power law for $Q > 0.07$ nm^{-1}). For fresh or partially dried suspensions with either pH 2 or pH 9, the organization of primary particles is predominantly chainlike with a power law exponent of 1.2 ± 0.1. For the fully dried suspensions the exponent is less well-defined and the mean exponent for the pH 2 and pH 9 fully dried suspensions is 1.4 ± 0.2. In contrast, the freshly made pH 8 suspension exponent in this Q range is 1.9 ± 0.1, clearly indicating the presence of sheetlike structures. The specificity of a strong sheetlike aggregation mechanism to this one pH suggests that it is correlated with the presence of the isoelectric point near the same pH. Unfortunately, no USAXS data were obtained for the partially dried pH 8 suspensions, but on fully drying, the sheetlike structure disappears [Fig. 6(c)] and

the exponent is not significantly different from that for pH 2 or pH 9. This is understandable from the standpoint that decreasing separation of the sheets probably occurs during drying (presumably the sheets are held apart by intervening water layers), and some rumpling occurs as well. Once the sheet thickness becomes larger than the sheet separation distance (e.g., through stacking of thinner sheets, through rumpling in the thickness direction, or through growth), USAXS no longer quantifies the structural unit as a sheet. However, it is clear from SEM pictures of pH 8 dried suspensions (Figs. 4 and 5) that the sheetlike morphology originally present in suspension is captured on drying as sheetlike layers within very large particles. SEM pictures indicate some sheetlike structure is also present in the final dried aggregates at pH 9; however, judging from the USAXS data, these sheets were not as cleanly resolved in suspension as were those at pH 8. In fact, some sheetlike structure is suggested in the USAXS data for the partially dried pH 2 suspension. Whether these observations are due to rumpling in the suspensions or a mixed assembly mode in suspension (partial chain + partial sheet construction of agglomerates) is unclear.

3. Large scale agglomerate structure

A steeper power law in Q is observed for $Q < 0.07$ nm^{-1}, meaning that structural arrangement at the largest length-scales (>80 to 100 nm) is different from that in the intermediate scale regime just described. In the >80 to 100 nm size range, chain- and sheetlike structures give way to more three-dimensional shapes, either with rough or smooth surfaces. In the pH 2 and pH 9 fresh suspensions a surface-fractal $Q^{-3.8}$ power law is observed with the exponent 3.8 ± 0.1, corresponding[18,21] to a surface-fractal exponent, D_S, of 2.2 ± 0.1. On partial drying, the exponent changes to 3.4 ± 0.2 corresponding to increased surface roughness with $D_S = 2.6 \pm 0.2$. However, on fully drying, almost pure Porod scattering is recovered: $Q^{-3.9}$ scattering, with the exponent 3.9 ± 0.1. For the fresh pH 8 suspension, no surface-fractal power law is observed. Instead the data at $Q < 0.07$ nm^{-1} exhibit a volume- or mass-fractal scaling law[18] ($Q^{-2.6}$) that could be associated with the void space within crumpled stacks of sheets, as has been found previously in some clay systems.[21] No data were obtained for the partially dried suspension, but after fully drying, the mass-fractal scaling law has disappeared and has been replaced by the same almost pure Porod scattering as for the dried pH 2 and pH 8 suspensions.

4. Structural changes on full drying

The Q^{-4} Porod law is associated with a smooth surface (i.e., a surface that is neither rough nor diffuse). The fact that all large aggregates attain such smooth surfaces on drying, regardless of pH, indicates that the driving force for the "smoothing" of the surface is not pH or pH-dependent phenomena such as dissolution or electrostatic forces. A plausible explanation is that capillary stresses arise in the final stages of drying, as air–water interfaces are generated inside the agglomerates, and that this tends to pull stray particulate clusters or fibrils at the outer fringes of each large agglomerate back onto the agglomerate surface proper [Figs. 7, dried state]. In the pH 8 case, a similar event occurs across the outer surfaces of each stack of plates. The end effect would be a smoother surface, regardless of pH. As discussed earlier, the intermediate-scale chainlike structures appear not to be affected significantly on drying (Fig. 7). This is an indirect observation of the strength of the inner agglomerate structure, given that both capillary and drying stresses can reach tens or hundreds of MPa in nanoparticulate bodies, as discussed in Sec. I. Finally, the intermediate sheetlike structures seen at pH 8 do appear to collapse upon each other as water is removed and may rumple as well. Primary particles, at the smallest size scale, lose their gellish outer layer, which may correspond to the loss of the electrostatic double layer.

These observations of agglomerate structure during the final stages of drying suggest a minimal role of capillary stress: some sheet rumpling and some smoothing of

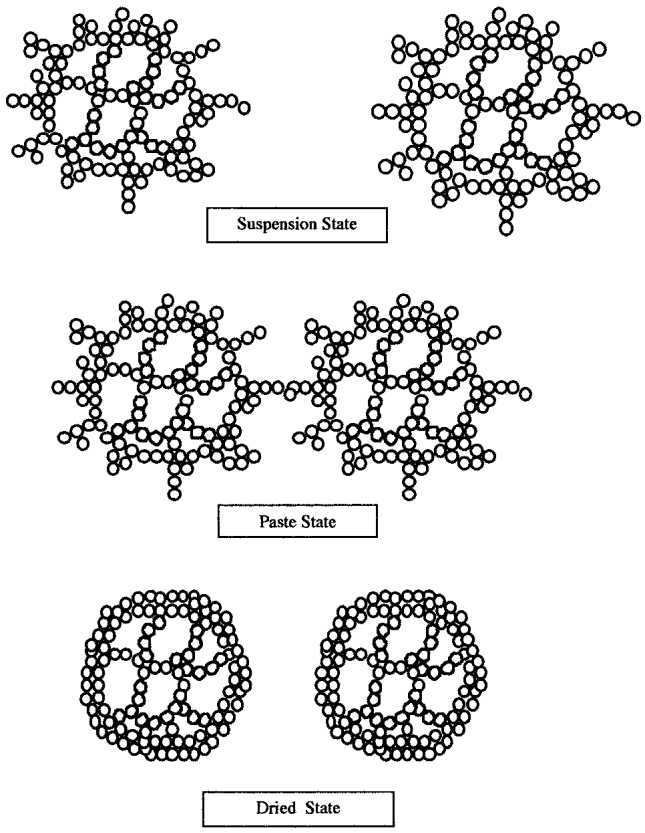

FIG. 7. Model of agglomerate structure consistent with USAXS data, applicable to both pH 2 and pH 9 agglomerates.

external surfaces of large agglomerates. Strikingly notable is the fact that large agglomerates (at least 1.5 μm in size, which is the USAXS detection limit, corresponding to a Q of 0.0015 nm^{-1}, Fig. 6) appear well before air-water interfaces are introduced into the system. Recall that these large agglomerates were not observed in the initial dilute SEM suspensions, but are observed in initial USAXS suspensions. Because the primary difference between these two suspensions is their level of particle concentration, not the presence or absence of an air–water interface, the results suggest that capillary/water tension forces are not necessary for large agglomerate formation. Possible mechanisms for agglomerate formation between the dilute and concentrated suspension state are given below.

5. Difference in agglomerate structure as seen in USAXS versus SEM

The SEM pictures of suspended powders (Fig. 1) and the USAXS data from suspended powders (Fig. 6) present qualitatively different views of the state of agglomeration in suspension. The SEM pictures show small agglomerates, highly isolated and mostly globular at all pH values. The USAXS data present a much more complex picture, with sophisticated agglomerate structures and much larger agglomerates present. The difference between the two views can be explained on the basis of the suspension concentration used in the two experiments. For the SEM experiments, extremely dilute (0.01% mass fraction, 0.0016% volume fraction) suspensions were used, as it was necessary to capture discrete, well-separated particles on the grid and not a mass of unresolvable powder. The USAXS studies were carried out on much more highly concentrated suspensions (3–25% volume fraction or 15–66% mass fraction in the case of zirconia) to obtain acceptable counting statistics. The factor of 600 to 15,000 increase in concentration in the USAXS samples significantly increases the probability of agglomerate formation for two reasons.

First, the higher volume fraction of particles in USAXS suspensions should lead directly to a greater frequency of particle–particle interaction and thus a much faster rate of agglomeration[22,23] than in the SEM experiments of Fig. 1. Secondly, as demonstrated by the zeta potential measurements, a high concentration of dissolved ions effectively eliminates the long-range repulsive forces present between particles. In practice, high concentrations of dissolved ions can occur either through initially high powder loading (as in the USAXS case) or through water removal from more dilute suspensions as they dry. Short-range interparticle forces will then dominate in high ionic strength suspensions; these encompass primarily attractive forces, e.g., London–Van der Waals forces and (potentially) ion–ion correlation forces.[24] The latter forces are similar to Van Der Waals forces, in that they involve correlated dipole–dipole interactions, but the dipoles in question are not comprised of the electrons around an atom, but rather, the sheath of dissolved ions around a small particle. Both forces would tend to be particularly enhanced in the presence of dissolved $Y^{+3,}$ due to its large charge-to-size ratio. High Y^{+3} concentrations would tend to both collapse the double layer of ions around a particle (thereby decreasing the interparticle separation distance and increasing London–Van der Waals attractive forces) and yield a high spatial charge density of the ion cloud for dipole interactions.[24] The net result would be an increased tendency for agglomeration in any suspension with high dissolved ion content, i.e., regardless of pH or zeta potential. This is, in fact, what is observed in the present USAXS study.

The observations of the present study indicate that merely concentrating yttria–zirconia suspensions may be enough to induce agglomeration. For this reason, there is little hope—at least in the present system—for obtaining agglomerate-free slurries or powders by drying from agglomerate-free, ultra-dilute suspensions. Additionally, it will be very difficult to disperse powders into a high solids loading suspension; due to high dissolved ion content, there may well be insufficient repulsive forces to assist dispersion in the first place—or, if dispersion does occur, agglomerates will then reform due to particle impacts in almost zero time.

One can expect that agglomeration would continue to increase as the concentration of ions and particles becomes ever greater during drying. The logical terminal end of this drying process is the formation of the multi-micron-sized particles seen in SEM of dried powders (Figs. 4 and 5). As noted earlier, the underlying arrangement of crystallites within agglomerates has seen little change throughout drying, except where the pH is close to the isolectric point. The USAXS sequence in Figs. 6 and 7 illustrates this point, showing the same 3-stage hierarchical arrangement of primary particles all the way from the concentrated suspension state, through the partially dried paste state, through final drying. With a minimum measurable Q of 0.0015 nm^{-1}, the present USAXS studies cannot detect any size increase of agglomerates larger than about 1.5 μm; thus it is not known whether the very largest granules and agglomerates in SEM images were already present in the concentrated USAXS suspensions (before complete drying) or not. This is an area for future work, possibly accessible by liquid cell computed x-ray microtomography.

6. Mechanism of structure development in agglomerates

It is important to note that while the length scale of the interparticle repulsion may be decreased in concentrated suspensions (due both to consolidation of a particle's double layer in suspensions of high ionic strength, and

the shielding provided by the surrounding ions), it is not completely absent. The fact that distinctly different structures are observed at the isoelectric point than occur away from it (on both sides) would indicate that surface charge does play some role in agglomerate formation. Furthermore, the nature of the observed agglomerate geometries is consistent with a charged particle scenario. Away from the isoelectric point, the primary particles (crystallites) are highly charged and thus can withstand close approach without attachment. Agglomerates grow through the eventual attachment of particles that are highly mobile throughout much of their approach. Each primary particle has the opportunity to seek a low energy site for attachment, resulting in a fairly dense close-packing arrangement of chains within the growing agglomerate, which may nevertheless have a fractally rough surface. Agglomerate growth is attachment/reaction-limited. In contrast, primary particles at the isoelectric point are sticky and attach at the first point of contact with the growing agglomerate. The result is a planar structure, consistent with diffusion (mobility)-limited growth. If individual planes stack before becoming rumpled, a porous lamellar structure can be formed that contains a volume-fractal internal void morphology, such as occurs in clays and porous rocks.[21] This structural development is also analogous to the growth of metallurgical phases by atom attachment; reaction (attachment)-limited growth results in the formation of equiaxed phase morphologies, while diffusion-limited growth (such as that encountered during the freezing of a eutectic melt) results in the formation of lamellar structures.[25]

7. Summary of USAXS data

To summarize the USAXS data, the fresh suspensions exhibit two distinct particle morphologies. Away from the isoelectric point primary particles have a diffuse or gellish interface with the aqueous suspension medium, organize predominantly into chains in the nano-to-mesoscale regime, and coalesce into larger agglomerates with fractally rough surfaces. On drying the primary particle surfaces become less diffuse, and the fractal roughness of the agglomerates is first accentuated. However, on fully drying, the large-scale agglomerate surfaces become smooth and the primary particle surfaces become sharply defined. The chainlike structure at intermediate length scales mainly persists through the end of drying, in defiance of significant capillary forces. In contrast at the isoelectric point, primary particles have a sharp interface with the aqueous suspension medium, organize predominantly into sheets in the nano-to-mesoscale regime, and coalesce into larger porous agglomerates in which either the porosity or the solid phase exhibits volume- or mass-fractal characteristics. While no data are available for partial drying, full drying has the effect of removing the volume-fractal and sheetlike structures and replacing them with the same surface-fractal and chainlike structures as observed for fully dried suspensions with pH away from the isoelectric point.

IV. SUMMARY AND CONCLUSIONS

Results from the SEM, USAXS, zeta potential, and dissolution studies suggest the following picture of agglomerate formation in the YSZ suspensions. First, dissolution/reprecipitation plays a minor role. There appears to be no significant increase in the number and size of agglomerates present when dissolution of Y is increased by four orders of magnitude over the pH 9 to pH 2 range. Reprecipitation of dissolved matter at interparticle necks would be expected to measurably decrease the surface area per unit mass as drying proceeds, but this is also not detected in the present experiments. Whether more minor reprecipitation of dissolved matter can strengthen agglomerate networks already formed by other means is not addressed in the present work. However, other studies, including some using the present powder, indicate such is indeed the case.[2,15]

Second, capillary forces are not implicated in agglomerate formation. An order of magnitude increase in agglomerate size is observed just in going from dilute to concentrated suspensions, before air–water interfaces are introduced. It appears that the degree of suspension concentration alone can drive the formation/retention of large agglomerates. Possible reasons for this effect include the increased opportunity for particle–particle interaction with increasing particulate concentration, and also the diminished range of electrostatic repulsive forces that occurs as dissolved ions (from the particulate material itself, or from surface contaminants) become increasingly concentrated in the little remaining water. Capillary forces may play a secondary role in the assimilation of small agglomerates into larger ones; this was not directly detected in these experiments except as a diminution in the surface roughness of large agglomerates in the last stage of drying.

Finally, while dissolution and capillary forces both play a minimal role in agglomerate formation, there appears to be a significant contribution from zeta potential. The high ion concentration conditions that lead to agglomerate formation, as described above, are also low zeta potential conditions. Furthermore, purposeful changes in zeta potential lead to demonstrably different agglomerate structures. Sheetlike structures form near the isoelectric point (zeta potential = 0), while globular structures form away from the isoelectric point. The globular versus layering morphology seen at the nanoscale in USAXS is also observed at micron and larger scales in SEM of dried suspensions, thereby indicating that the fundamental mechanism of agglomerate growth

does not change with either degree of drying or size scale. In the case of the sheetlike structures, it is hypothesized that a mobility-limited growth mechanism is operating, while the globular structures may evolve from attachment-limited growth.

While a fully quantitative interpretation model has yet to be developed for these data, USAXS studies show the connection between agglomeration processes over a wide range of both length-scale and concentration of nanoparticulate suspensions.

ACKNOWLEDGMENTS

This work was supported by the Office of Naval Research under Contract No. N00014-98-1-0637 and by the Particulate Materials Center at the Pennsylvania State University. We acknowledge Jan Ilavsky [National Institute of Standards and Technology (NIST)/University of Maryland], Pete Jemian and Paul Zschack [University of Illinois/University-National Laboratory-Industry Collaborative Access Team (UNICAT)] for scientific and technical support for the USAXS measurements. The UNICAT facility at the Advanced Photon Source (APS) is supported by the University of Illinois at Urbana/Champaign, Materials Research Laboratory [United States Department of Energy (U.S. DOE), the State of Illinois, Illinois Board of Higher Education-Higher Education Cooperation Grant (IBHE-HECA)], Oak Ridge National Laboratory (U.S. DOE), NIST (U.S. Department of Commerce), and UOP Limited Liability Corporation (LLC). Use of the Advanced Photon Source was supported by the U.S. DOE, Office of Science, Office of Basic Energy Sciences, under Contract No. W-31-109-ENG-38. The authors express their appreciation to Sean Sweeney of Pennsylvania State University for zeta potential measurements in suspensions having concentrated filtrate.

Information on commercial products is given for completeness and does not constitute or imply their endorsement by the National Institute of Standards and Technology.

REFERENCES

1. S. Kwon and G.L. Messing, Nanostruct. Mater. **8,** 399 (1997).
2. A. Maskara and D.M. Smith, J. Am. Ceram. Soc. **80,** 1715 (1997).
3. T.C. Patton, *Paint Flow and Pigment Dispersion* (John Wiley and Sons, New York, NY, 1979), p. 266.
4. G.W. Scherer, J. Am. Ceram. Soc. **73,** 3 (1990).
5. M. Çiftçioglu and M.J. Mayo, in *Superplasticity in Metals, Ceramics, and Intermetallics,* edited by M.J. Mayo, M. Kobayashi, and J. Wadsworth (Mater. Res. Soc. Symp. Proc. **196,** Pittsburgh, PA, 1990) pp. 77–86.
6. B.D. Cullity, *Elements of X-Ray Diffraction* (Addison-Wesley Publishing Co., Reading, MA, 1967), p. 99.
7. G.G. Long, P.R. Jemian, J.R. Weertman, D.R. Black, H.E. Burdette, and R.D. Spal, J. Appl. Crystallogr. **24,** 30 (1991).
8. G.G. Long, A.J. Allen, J. Ilavsky, P.R. Jemian, and P. Zschack, in *Synchrotron Radiation Instrumentation: 11th U.S. National Conference,* edited by P. Pianetta, J. Arthur, and S. Brennan (American Institute of Physics Conf. Proc. **521,** Melville, NY, 2000), pp. 183–187.
9. J.A. Lake, Acta Crystallogr. **23,** 191 (1967).
10. J.A. Potton, G.J. Daniell, and B.D. Rainford, J. Appl. Crystallogr. **21,** 663 (1988).
11. G. Porod, in *Small-Angle X-ray Scattering,* edited by O. Glatter and O. Kratky (Academic Press, London, U.K., 1982), pp. 17–51.
12. Douglas A. Skoog and James J. Leary, *Principles of Instrumental Analysis*, 4th ed. (Harcourt Brace College Publishers, Fort Worth, TX, 1992), p. 223.
13. J.H. Adair, H.G. Krarup, S. Venigalla, and T. Tsukada, in *Aqueous Chemistry and Geochemistry of Oxides, Oxyhydroxides, and Related Materials,* edited by J.A. Voigt, T.E. Wood, B.C. Bunker, W.H. Casey, and L.J. Crossey (Mater. Res. Soc. Symp. Proc. **432,** Pittsburgh, PA, 1997), pp. 101–112.
14. R.N. Basu, C.A. Randall, and M.J. Mayo, J. Am. Ceram. Soc. **84,** 33 (2001).
15. A. Vertanessian, M.S. Thesis, The Pennsylvania State University, University Park, PA (2001).
16. B. Mittal, V.M. Puri, and C.F. Mancino, ASAE Meeting Presentation Paper No. 004011 (2000), available at http://www.asae.org.
17. M.J. Mayo and M. Çiftçioglu, in *Clusters and Cluster-Assembled Materials,* edited by R.S. Averback, D.L. Nelson, and J. Bernholc (Mater. Res. Soc. Symp. Proc. **206,** Pittsburgh, PA, 1991), pp. 545–550.
18. G. Beaucage, *J. Appl. Crystalogrl.* **29,** 134 (1996).
19. S. Ross and I.D. Morrison, *Colloidal Systems and Interfaces* (John Wiley & Sons, New York, NY, 1988), p. 233.
20. Akash and M.J. Mayo, J. Am. Ceram. Soc. **82,** 2948 (1999).
21. A. J. Allen, J. Appl. Cryst. **24,** 624 (1991).
22. R.J. Hunter, *Foundations of Colloid Science* (Oxford University Presss, Oxford, U.K., 1986), pp. 92–94, 440–447.
23. C. Stainton, W. Liang, and K. Kendall, Eng. Fract. Mech. **61,** 83 (1998).
24. G.V. Franks, S.B. Johnson, P.J. Scales, D.V. Boger, and T.W. Healy, Langmuir **15,** 4411 (1999).
25. R.E. Reed-Hill and R. Abbaschian, *Physical Metallurgy Principles*, 3rd ed. (PWS-Kent Publishing Company, Boston, MA, 1992), p. 474.